Muscle mitochondrial catalase expression prevents neuromuscular junction disruption, atrophy, and weakness in a mouse model of accelerated sarcopenia

Hongyang Xu[1], Rojina Ranjit[1], Arlan Richardson[2,3] & Holly Van Remmen[1,3]* iD

[1]*Aging & Metabolism Research Program, Oklahoma Medical Research Foundation, Oklahoma City, OK, USA;* [2]*Department of Biochemistry & Molecular Biology, University of Oklahoma Health Sciences Center, Oklahoma City, OK, USA;* [3]*Oklahoma City VA Medical Center, Oklahoma City, OK, USA*

Abstract

Background Oxidative stress and damage are associated with a number of ageing phenotypes, including age-related loss of muscle mass and reduced contractile function (sarcopenia). Our group and others have reported loss of neuromuscular junction (NMJ) integrity and increased denervation as initiating factors in sarcopenia, leading to mitochondrial dysfunction, generation of reactive oxygen species and peroxides, and loss of muscle mass and weakness. Previous studies from our laboratory show that denervation-induced skeletal muscle mitochondrial peroxide generation is highly correlated to muscle atrophy. Here, we directly test the impact of scavenging muscle mitochondrial hydrogen peroxide on the structure and function of the NMJ and muscle mass and function in a mouse model of denervation-induced muscle atrophy CuZnSOD (*Sod1*$^{-/-}$ mice, *Sod1*KO).

Methods Whole-body *Sod1*KO mice were crossed to mice with increased expression of human catalase (MCAT) targeted specifically to mitochondria in skeletal muscle (mMCAT mice) to determine the impact of reduced hydrogen peroxide levels on key targets of sarcopenia, including mitochondrial function, NMJ structure and function, and indices of muscle mass and function.

Results Female adult (~12-month-old) *Sod1*KO mice show a number of sarcopenia-related phenotypes in skeletal muscle including reduced mitochondrial oxygen consumption and elevated reactive oxygen species generation, fragmentation, and loss of innervated NMJs ($P < 0.05$), a 30% reduction in muscle mass ($P < 0.05$), a 36% loss of force generation ($P < 0.05$), and a loss of exercise capacity (305 vs. 709 m in wild-type mice, $P < 0.05$). Muscle from *Sod1*KO mice also shows a 35% reduction in sarco(endo)plasmic reticulum ATPase activity ($P < 0.05$), changes in the amount of calcium-regulating proteins, and altered fibre-type composition. In contrast, increased catalase expression in the mMCAT × *Sod1*KO mice completely prevents the mitochondrial and NMJ-related phenotypes and maintains muscle mass and force generation. The reduction in exercise capacity is also partially inhibited (~35%, $P < 0.05$), and the loss of fibre cross-sectional area is inhibited by ~50% ($P < 0.05$).

Conclusions Together, these striking findings suggest that scavenging of mitochondrial peroxide generation by mMCAT expression efficiently prevents mitochondrial dysfunction and NMJ disruption associated with denervation-induced atrophy and weakness, supporting mitochondrial H_2O_2 as an important effector of NMJ alterations that lead to phenotypes associated with sarcopenia.

Keywords Skeletal muscle; Mitochondria; Neuromuscular junction; ROS; Oxidative stress; Catalase; *Sod*

Introduction

Oxidative stress is commonly defined as the imbalance between the generation of pro-oxidants and antioxidant defence resulting in an accumulation of oxidized or damaged molecules. In skeletal muscle, increased oxidative stress is closely associated with a number of negative phenotypes including loss of muscle mass and contractile strength, disruption of neuromuscular junction (NMJ) integrity and function, damage to mitochondrial functions including a reduced oxygen consumption rate (OCR), and a higher production rate of reactive oxygen species (ROS).[1] Elevated oxidative stress in skeletal muscle has been implicated in a number of pathological conditions, such as muscle disuse, age-associated muscle loss in sarcopenia, denervation, muscular dystrophies, and cancer cachexia.[2] A major source of cellular oxidative stress is mitochondrial electron transport chain generation of superoxide anions and hydrogen peroxide.[3]

To study the impact of increased oxidative stress in sarcopenia, our group developed the *Sod1*KO mouse as an accelerated sarcopenia model that faithfully reproduces muscle and motor neuron phenotypes normally associated with age-related muscle atrophy and weakness but the onset is accelerated appearing in younger adult mice. *Sod1*KO mice lack CuZnSOD, a primarily cytosolic superoxide dismutase that converts superoxide anion to hydrogen peroxide, and exhibit a number of oxidative stress-induced phenotypes, including accelerated loss of muscle mass and weakness, altered NMJ function and morphology, and mitochondrial dysfunction (reduced oxygen consumption, ATP production calcium buffering capacity, and increased production of H_2O_2 and lipid hydroperoxides.[1,4,5] Importantly, in human subjects, the antioxidant enzyme CuZnSOD has been found to be closely associated with sarcopenia, in that the content and activity of CuZnSOD are dramatically reduced in sarcopenic patients.[6] Our studies in this model and mouse models designed to target deletion of CuZnSOD to either motor neurons or skeletal muscle have led us to hypothesize that loss of innervation induces muscle mitochondrial generation of both H_2O_2 and lipid peroxides, contributing to a significant loss of muscle function and atrophy.[5] In this study, we have targeted removal of muscle mitochondrial electron transport chain-derived generation of H_2O_2 in the *Sod1*KO mouse model using muscle-specific expression of a mitochondrial-targeted H_2O_2 scavenger, human catalase (mMCAT).

Catalase is a peroxisomal antioxidant enzyme that catalyzes the decomposition of hydrogen peroxide generated by oxidation of a number of substrates including long-chain fatty acids. A whole-body mitochondrial catalase transgenic mouse (MCAT mice) was generated a decade and a half ago[7] using a mitochondrial targeting sequence to direct the expression of the transgene specifically to the mitochondria where it could scavenge hydrogen peroxide generated by the electron transport chain. The MCAT mice displayed a significant enhancement of mitochondrial function, that is, reduced ROS production and energy imbalance.[7] Global expression of MCAT has been shown to improve muscle function in mice, including enhanced exercise ability and improved maximum specific force, and also results in reduced pathology in other disease models.[8] The tissue-specific (MCAT) transgenic mouse model utilized here is a unique tool that allowed us to generate skeletal muscle-specific expression through removal of a stop codon in the transgene under direction of a tissue-specific Cre recombinase to generate the mMCAT model.[9] The mMCAT mice were crossed to the *Sod1*KO mice to determine whether scavenging muscle mitochondrial H_2O_2 would alter the sarcopenia phenotypes present in the *Sod1*KO mice.

Our results clearly show that muscle-specific mitochondrial expression of catalase is sufficient to prevent NMJ disruption and the associated muscle atrophy and weakness phenotypes in the *Sod1*KO mice, supporting an important role for muscle–neuron crosstalk and for maintaining muscle mitochondrial H_2O_2 in preventing deleterious muscle phenotypes associated with sarcopenia.

Materials and methods

Generation of the whole-body CuZnSOD knockout (Sod1KO) mice and the muscle-specific mitochondrial-targeted catalase (mMCAT) transgenic mice

The *Sod1*KO mice used in this study were maintained on a C57BL/6J background. The mice were originally generated by Dr Charles Epstein's laboratory at the University of California San Francisco, and the details have previously been reported.[4] Mitochondrial-targeted catalase (MCAT) flox mice were developed by inserting a human MCAT construct with a stop signal flanked by LoxP sites preceding the catalase gene between exons 2 and 8 of a human GAPDH bacterial artificial chromosome.[9] Acta Cre transgenic mice[10] (from JAX Stock No. 006149) were used to generate skeletal muscle-specific expression of the MCAT transgene through the removal of LoxP sites and the stop codon, allowing the expression of MCAT specifically in skeletal muscle (mMCAT mice). The expression of the ACTA Cre transgene is induced early in embryonic development[10]; thus, catalase expression was induced from early development as well. The mMCAT mice were bred to *Sod1*KO mice, to generate four groups of mice with different genotypes, wild-type (WT), WT/mMCAT, *Sod1*KO, and *Sod1*KO/mMCAT. Specifically, MCAT^flox/flox Acta Cre^+/o *Sod1*^−/− or MCAT^flox/flox Acta Cre^+/o *Sod1*^+/− male mice were

bred to MCAT$^{flox/flox}$ Acta Cre$^{o/o}$ *Sod1*$^{+/-}$ female mice to generate MCAT$^{flox/flox}$ Acta Cre$^{+/o}$ *Sod1*$^{-/-}$ (MCAT*Sod1*KO), and MCAT$^{flox/flox}$ Acta Cre$^{+/o}$ *Sod1*$^{+/+}$ (mMCAT Tg mice) and MCAT$^{flox/flox}$ Acta Cre$^{o/o}$ *Sod1*$^{+/+}$ (WT) female control mice. All mice were caged in a pathogen-free environment with free access to standard chow and water and maintained on a 12 h light/dark cycle, and measurements were performed in female mice at around 12 months of age, unless otherwise stated. The Institutional Animal Care and Use Committee at Oklahoma Medical Research Foundation (Oklahoma City, OK, USA) approved all procedures.

Assessment of muscle contractile properties, functional denervation, and neuromuscular junction (NMJ) function in situ

Isometric contractile force generation was measured *in situ* in gastrocnemius (GTN) muscle based on the methods described previously.[11] Briefly, mice were anaesthetized with isoflurane, and the whole GTN muscle was isolated and cleaned from surrounding muscles and connective tissues. After dissection, the isolated muscle was tied with silk suture on the distal tendon, and the tendon was severed and mounted onto the force transducer (Model 305B, Aurora Scientific). The mouse was placed on a temperature-controlled platform at 37°C and provided with continuous anaesthesia. The electrode was placed on the surface of GTN muscle directly, and the muscle optimal length was adjusted with single 0.2 ms stimulation pulses until a maximum twitch reached. At the muscle optimal length, a series of 300 ms stimulus pulses were applied to achieve the maximum isometric tetanic force. After muscle stimulation, the electrode was moved from muscle to the sciatic nerve, and the nerve filament hooked firmly by the electrode. The same pulses of tetanic stimulus were applied to the nerve to achieve the nerve-induced maximum isometric tetanic force. All of the earlier tetanic twitch protocols were repeated several times to confirm the reproducibility and reliability of the data. Comparing muscle and nerve stimulated contractile force generation allows us to measure the extent of function denervation or loss of contractile force generation due to loss of intact NMJ innervation.

After all force measurements were completed, muscles were carefully removed and weighed, and the maximum tetanic force was normalized to the muscle cross-sectional area (CSA) calculated by the length and weight of the GTN muscle (dividing the muscle mass, mg, by the optimal length, mm, and the density of mammalian skeletal muscle, 1.06 g/cm^3) to give the specific force (N/cm^2). The NMJ function was presented by normalizing the nerve-induced force to the muscle-induced force as a percentage.

Measurement of mitochondrial respiration and reactive oxygen species (ROS) production

Mitochondrial function was measured in permeabilized muscle fibres. The permeabilization protocol has been previously described by our laboratory.[12] In general, a small piece of red GTN muscle was excised from the body and finely dissected to separate the muscle fibres along their striations in cold *buffer X* containing (in mM): 7.23 K$_2$EGTA, 2.77 CaK$_2$EGTA, 20 imidazole, 0.5 DTT, 20 taurine, 5.7 ATP, 14.3 PCr, 6.56 MgCl$_2$·6H$_2$O, and 50 K-MES (pH 7.1); 30 μg/mL saponin was added to the fibres to induce permeabilization for 30 min, followed by 5 min washes for three times in washing buffer containing (in mM): 105 K-MES, 30 KCl, 10 K$_2$HPO$_4$, 5 MgCl$_2$·6H$_2$O, 0.5 mg/mL BSA, and 0.1 EGTA (pH 7.1). After washing, the permeabilized fibres were placed into the Oxygraphy-2K (O2k, Oroboros Instruments, Austria) following the protocols described before.[13] The OCR was determined using the oxygen probe, while the ROS production rate was measured by the O2K-Fluo LED2-Module Fluorescence-Sensor Green with Amplex UltraRed Reagent (Invitrogen, A36006). In a few random samples, 10 μM cytochrome *c* was added into the system to confirm the integrity of the mitochondrial outer membrane[14] (Supporting Information, *Figure* S4). An increase >15% is considered to be evidence of a compromised preparation. An H$_2$O$_2$ standard curve was measured each time before the actual experiments to calibrate the level of H$_2$O$_2$. All data generated from O2K were normalized to the muscle wet weights and analysed with the official O2K software, DataLab Version 7.0.

Sarco(endo)plasmic reticulum ATPase (SERCA) activity assay

The sarco(endo)plasmic reticulum ATPase (SERCA) enzyme activity was measured in muscle homogenates at 37°C using a spectrophotometric assay as previously described.[15] In brief, all muscle samples were homogenized following the ratio 1:10 with the SERCA homogenizing buffer, containing (in mM): 250 sucrose, 5 HEPES, 0.2 PMSF, and 0.2% NaN$_3$. After centrifugation of the homogenates, the supernatant was taken with the protein amount of 100 μg and mixed with the SERCA assay buffer containing (in mM) 200 KCl, 20 HEPES, 10 NaN$_3$, 1 EGTA, 15 MgCl$_2$, 5 ATP, and 10 phosphoenolpyruvate, to generate a 3 mL mixture. At this point, 18 U/mL of lactate dehydrogenase and pyruvate kinase (PK/LDH) and 1 mM Ca^{2+} ionophore A-23187 (C-7522; Sigma) were added into the mixture. This reaction mixture was aliquoted and mixed with CaCl$_2$ to form eight different calcium concentrations with pCa points from 7.6 to 4.2 and a blank and then loaded into a pre-warmed 37°C quartz plate. The reaction was initiated by adding 1 mM NADH into the mixture, and the kinetic assay was performed by the following settings:

temp = 37°C, time = 30 min, λ = 340 nm, and shaking between readings. The SERCA activity was calculated using the formula

$$\text{Total ATPase rate} = \frac{\text{rate of } A_{340\text{ nm}} \text{ signal loss}}{\text{pathlength} * 6.23 \text{ mM/cm}}$$

Muscle myosin heavy chain (MHC) composition assay

Skeletal muscle myosin heavy chain (MHC) composition was determined by distinguishing all four MHC isoforms, MHCIIa, MHCIIx, MHCIIb, and MHCI. In this study, GTN muscle samples were homogenized and denatured as described previously.[16,17] Then the denatured muscle sample was separated with a special SDS-PAGE gel, the separating gel consisted of 32% v/v glycerol, 8% w/v acrylamide with a 50:1 ratio of acrylamide to $N\prime$-ethylenebisacrylamide or Bis, 0.2 M Tris–HCl (pH 8.8), 0.1 M glycine, 0.4% w/v SDS, 0.1% w/v ammonium persulfate, and 0.05% v/v $N,N,N\prime,N\prime$-tetramethylethylenediamine (TEMED). The stacking gel comprised 32% v/v glycerol, 4% w/v acrylamide, and Bis at the same ratio (50:1) to acrylamide, 70 mM Tris–HCl (pH 6.7), 4 mM EDTA, 0.4% w/v SDS, 0.1% w/v ammonium persulfate, and 0.05% v/v TEMED. The gel was then run using two different buffers, the lower running buffer consisting of 0.05 M Tris (base), 75 mM glycine, and 0.05% w/v SDS, and the upper running buffer, which was at 6× the concentration of the lower running buffer and had β-ME added (final concentration: 0.12% v/v). The gel underwent electrophoresis at 150 V at 4°C for 24 h, and immediately after running, Coomassie Brilliant Blue G250 was used to stain the gel and visualize the MHC bands. The images were collected by G: BOX Chemi (Syngene, USA), and the densitometry analysis was conducted using ImageJ software (ImageJ, Fiji).

Histological staining

Muscle H&E staining
After the muscle was excised, it was placed in O.C.T mounting medium (Tissue-Tek, VWR, Radnor, PA, USA) and snap-frozen in isopentane pre-cooled in liquid nitrogen, so the myofibrils remained aligned properly. The muscle was cryosectioned into 8–10 μm cross-sections from the middle area of the whole muscle, and the muscle sections were then mounted onto slides. Slides were stained with the H&E staining kit from Thermo Fisher Scientific (Rapid Chrome H & E frozen section staining kit, #9990001), and then the slides were sealed with cover slips. Images were collected with Nikon Microphot-FXA microscope at ×20.

Immunohistochemistry staining for MHC isoforms
After collecting the muscle sections as described earlier, the sections were left at room temperature for ~10 min, and then the fixative (4% paraformaldehyde in PBS; PFA) was added onto the sections for 30 min. Afterwards, the fixative was washed off for 3 × 10 min by PBS, which was then followed by adding the immunobuffer (50 mM glycine, 0.033% saponin, 0.25% BSA, 5% corresponding serum same to secondary antibody host, and 0.05% sodium azide) onto the sections with incubating for 2 h at room temperature as described previously.[18] Then the immunobuffer-diluted primary antibody (MHCIIb (DSHB, BF-F3) with 1:20 dilution) was added onto the sections, and the sections were incubated for overnight at room temperature in an airtight, saturated container. After the primary antibody incubation, all slides were washed with immunobuffer followed by adding the secondary antibody (goat anti-mouse Alexa 647, Life Technology, #A21238) and incubating for 2 h in darkness. After the incubation, all slides were washed with PBS for 2 × 10 min and then sealed with coverslip under the presence of mounting medium (EMS, #17989). Immunofluorescent images were taken at the same magnificent (×20) with Nikon confocal microscope (Nikon Eclipse).

Confocal microscopy for NMJ morphology
After the muscle was excised from the body, small muscle pieces were taken under the cold PBS in a Petri dish along the fibre directions with a careful removal of fat and connective tissues. Muscle samples were transferred into a 24-well plate with 10% STUmol (Poly Scientific R&D, #2832) for 1 h to fix the tissue with gently shaking. After the fixation, washed tissues for 3 × 5 min in PBS at room temperature, and then permeabilized the tissue under the 2% Triton in PBS for 30 min on a shaker. After permeabilization, the tissues are placed into the blocking buffer containing, 4% BSA, 1% Triton, 5% serum matches the host of secondary antibody diluted in PBS, blocking for overnight in the cold room at 4°C. After blocking, primary antibodies, 1:50 SV2 (DSHB) for nerve terminals and 1:50 2H3 (DSHB) for neurofilaments, were added. The tissues were incubated overnight at 4°C, washed for 6 × 30 min in PBS at room temperature, and subsequently incubated with the secondary antibodies, 1:100 BTX-Alexa 488 (Invitrogen, #B13422), and 1:250 goat anti-mouse Cy3. After the incubation for secondary antibodies for overnight at 4°C, all tissues were then washed 6 × 30 min with PBS. Afterwards, tissues were transferred onto slides and mounted with mounting medium and sealed with nail polish. Images of NMJ were taken by the Nikon confocal microscope under the magnification of ×20, and Z-stacks were taken to show the 3D structure of intact NMJ. The total thickness of optical sections is around 20 to 60 μm, and the stack interval was set at every 1 to 2 μm, so there are around 20 to 30 images per stack.

The NMJ area was analysed as the area occupied by each individual-labelled AChR, and only the NMJs facing forward

were analysed. The fragmentation level was quantified by counting the fragmented pieces of each NMJ, and if there are five or more pieces per junction, the NMJ is considered as a fragmented NMJ. The denervation score was quantified as follows: Score 0: there is no denervation, the NMJ is fully overlapped with neural filament; Score 1: partial denervation, the NMJ is partially overlapped with neural filament; and Score 2: complete denervation, the NMJ has no overlap with neural filament. The statistical analysis for all images taken in this section was performed by ImageJ software (ImageJ).

Western blotting and antibody information

Gastrocnemius muscles were homogenized in RIPA buffer containing 50 mM Tris (pH 7.4), 150 mM NaCl, and protease inhibitors. Then the total protein was quantified with the Bio-Rad protein assay kit (Sigma-Aldrich, Poole, UK), and the same amount of protein was loaded and separated with SDS-PAGE gels at certain percentages, that is, 10% or 12%. The gel was then run at 200 V for 1 h and wet transferred onto 0.45 μm nitrocellulose membranes (Bio-Rad) with the conditions of 100 V, 30 min at 4°C, same as described before.[19] After the transfer of the gel, total proteins in each lane were quantified using Ponceau staining (Sigma, #P3504), and then the membrane was washed with ddH$_2$O to remove the Ponceau staining and blocked with 1% BSA solution in TBST for at least 1 h at room temperature. Soon after blocking, primary antibodies were added onto the membrane and incubated for overnight at 4°C. After the incubation of primary antibody, the membrane was washed with blocking buffer and then exposed to the secondary antibody for 30–60 min. After the secondary antibody, membrane was washed with TBST for the last time to clean the background. Protein bands were visualized and quantified using GeneTool system (SynGene, Frederick, MD, USA). The relative content of each protein measured using western blot analysis was normalized to sample total protein content measured using Ponceau stain and densitometry of total Ponceau in that sample lane. Primary antibody information was as follows: rabbit anti-*Sod1* (Enzo, #ADI-SOD-101-E), rabbit anti-human catalase (Athens Research & Technology, #0105030000), rabbit anti-GAPDH (Sigma, #9545), SERCA1 (DSHB, #CAF2-5D2), SERCA2 (Cell Signaling, 4388S), CSQ1/2 (Abcam, #ab3516), and parvalbumin (Abcam, #ab11427).

Statistical analysis

All results are presented as mean values ± standard deviation, and comparisons among different groups were performed with one-way ANOVA and Tukey's multiple-comparison test. The statistical analysis was undertaken by GraphPad Prism 8, and the statistical significance was set at P values <0.05.

Results

Validation of Sod1 deletion (Sod1KO) and muscle-specific expression of the human catalase transgene

The protein levels of CuZnSOD (~17 kDa) and mMCAT human catalase (~63 kDa) were determined by western blotting for all groups using whole GTN muscle homogenates. Lack of CuZnSOD expression was confirmed in *Sod1*KO groups (with and without mMCAT) (*Figure* 1A and 1B). Muscles from WT/mMCAT and *Sod1*KO/mMCAT mice clearly show a similar level of elevated expression of the human catalase transgene, and there is no detectable expression of human catalase in WT and *Sod1*KO groups (*Figure* 1A and 1C). It is important to note that we confirmed that no human MCAT expression is detected in tissues from other organs (*Figure* S3). Moreover, the western blot image with isolated mitochondria from GTN muscle shows that the expression of the human catalase is limited to mitochondria and is not present in the cytosol (*Figure* 1D). Thus, the *Sod1*KO/mMCAT mice have increased expression of catalase specifically in the muscle mitochondria.

Altered oxygen consumption rate (OCR) and peroxide generation in Sod1KO mice are reversed by mMCAT expression

We have previously reported functional defects of muscle mitochondria from *Sod1*KO mice.[1] In order to detect whether the expression of mMCAT in *Sod1*KO mice improves mitochondrial function, we measured the mitochondrial OCR and the ROS production rate as peroxide emission using permeabilized muscle fibres from red GTN muscle. Respiratory substrates were added to stimulate electron flow through different complexes (I, I + II, II, and IV), and fibres from the *Sod1*KO mice exhibited a lower OCR in all complexes compared with fibres from WT mice (*Figure* 2A). In contrast, the expression of mMCAT returned the OCR of all complexes in *Sod1*KO mice back to about the same level as seen in WT mice (*Figure* 2A). Moreover, in accordance with our previous findings, we found that the ROS production rate in State 1 respiration (mitochondria respiring without addition of external substrate) was significantly elevated in fibres from *Sod1*KO mice compared with fibres from WT mice (*Figure* 2B). mMCAT overexpression reduced ROS production rate in *Sod1*KO mice to the same level to WT mice (*Figure* 2B).
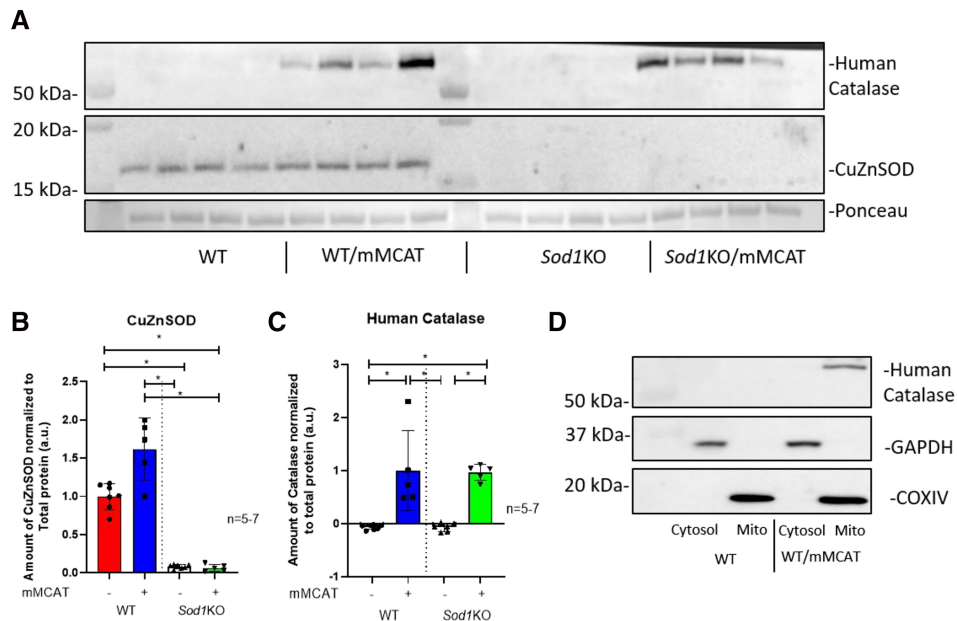
Figure 1 Validation of the deletion of *Sod1* and the skeletal muscle-specific transgene of mitochondrial catalase in gastrocnemius muscle homogenates. (*A*) Representative western blot and the pooled data for (*B*) CuZnSOD and (*C*) human catalase. (*D*) Representative western blot in isolated mitochondria and cytosol from WT and WT/mMCAT muscles, showing the mitochondrial specificity of the mMCAT human catalase transgene. *Significant difference between the labelled groups (*P* < 0.05, one-way ANOVA). *N* = 5–7, indicating the number of animals. Data are presented as mean value ± standard deviation.
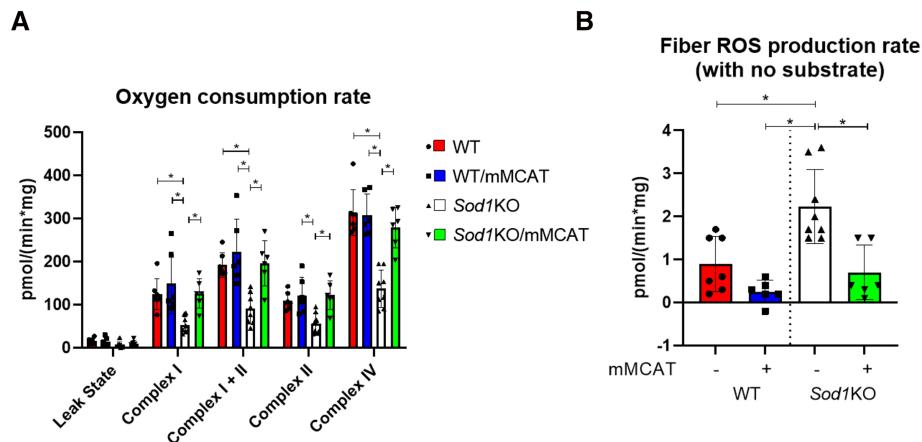

Figure 2 Detection of mitochondrial function. (*A*) Respiratory rate (oxidation–phosphorylation rate) substrates used for different complexes added sequentially. Leak state: 10 mM glutamate and 2 mM malate with no ADP; complex I: addition of 2.5 mM ADP; complex I + II: addition of 10 mM succinate; complex II: addition of 0.5 μM rotenone; and complex IV: addition of 2 mM ascorbate and 0.5 mM TMPD added after 5 μM antimycin A. (*B*) Reactive oxygen species (ROS) production rate of fibres with no substrate. *Significant difference between the labelled groups (*P* < 0.05, one-way ANOVA). *N* = 4–7, indicating the number of animals. Data are presented as mean value ± standard deviation.

Expression of the mMCAT transgene prevents changes in body composition and muscle atrophy and improves running capacity in Sod1KO mice

The measurement of body composition using quantitative magnetic resonance in the 12- to 14-month-old female *Sod1*KO mice revealed a significantly lower fat mass (~17%)

compared with WT mice (~31%) (*Figure* 3A). The expression of mMCAT in the *Sod1*KO mice is associated with a level of fat mass in the normal control range (~32%) (*Figure* 3A). In agreement with our previous findings, we also found a significant decline in the absolute muscle mass of the GTN muscle (~46%, *Figure* 3B). When normalized to the body mass, the normalized muscle mass was also found to be significantly
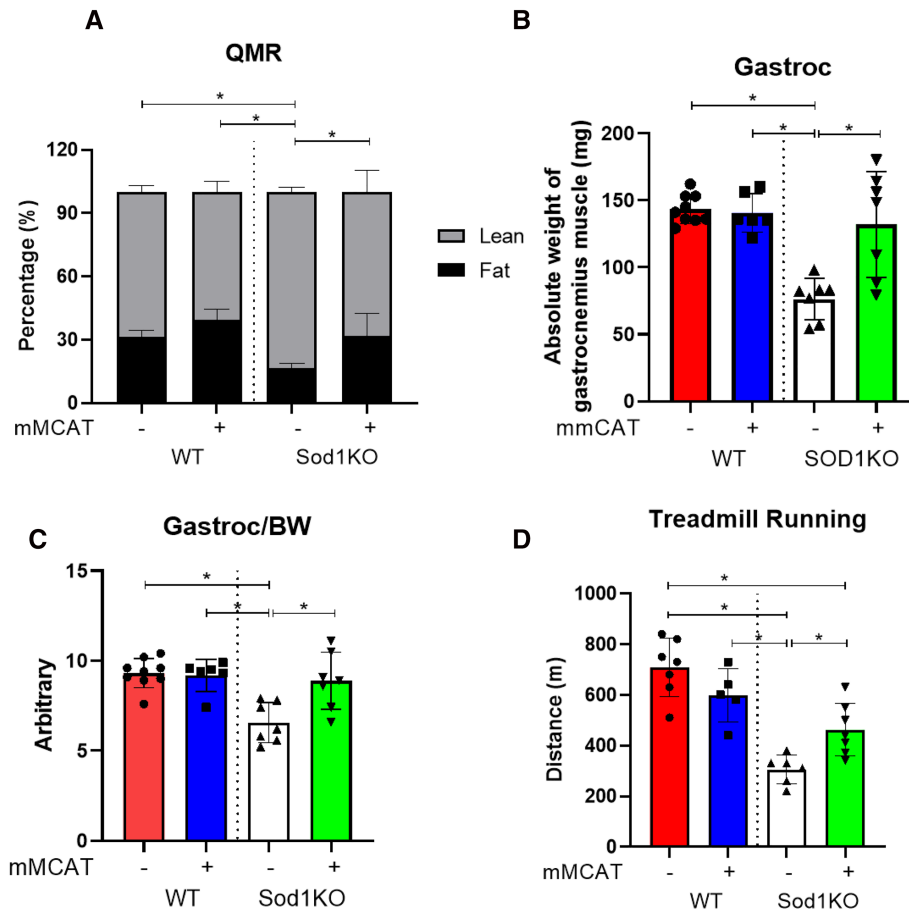
Figure 3 Body and muscle index and the exercise ability. (*A*) Overall body index, (*B*) absolute muscle weight, and (*C*) muscle/body weight. (*D*) Treadmill running exercise ability showing the distance to exhaustion in metres. *Significant difference between the labelled groups (*P* < 0.05, one-way ANOVA). *N* = 5–8, indicating the number of animals. Data are presented as mean value ± standard deviation.

decreased (~30%) in *Sod1*KO mice as compared with WT mice (*Figure* 3C). However, in *Sod1*KO mice with mMCAT expression, both absolute and relative muscle mass in the *Sod1*KO mice was restored to the same level as in the WT mice (*Figure* 3B and 3C). Performance on a treadmill revealed that the running ability (distance to exhaustion) is significantly lower in *Sod1*KO compared with WT mice (305 vs. 709 m) but restored by ~35% to 463 m with the expression of mMCAT (*Figure* 3D).

Fibre composition and diameter in Sod1KO mice are modified by mMCAT

Muscle fibre type is categorized by the MHC isoforms present. There are four different MHC isoforms present in adult mouse skeletal muscle, MHCI, MHCIIa, MHCIIx, and MHCIIb. The predominant isoforms in GTN muscle are the fast isoforms, MHCIIa, MHCIIx, and MHCIIb, and a small amount of the slow isoform MHCI. Because they have

different molecular weights, all MHC isoforms can be separated by SDS-PAGE gel. In comparison with WT mice, there is a dramatic alteration in MHC composition in *Sod1*KO mice, in that the abundance of MHCIIb fibres is decreased approximately 50%. The level of MHCIIb fibres is restored by the presence of mMCAT to a level similar to WT mice, while the amount of MHCIIa and IIx remained the same (*Figure* 4A and 4B).

We also measured the CSA by H&E staining (*Figure* 4C). The statistical analysis shows that fibre diameter is ~20% smaller in muscle from *Sod1*KO mice compared with WT mice, and the reduced fibre size in *Sod1*KO mice is partially reversed by mMCAT expression, resulting in only a 10% smaller fibre size compared with WT mice (*Figure* 4D). Confocal images with MHCIIb staining indicate a significant reduction of CSA in MHCIIb fibres from *Sod1*KO mice (17%), which approximates the reduction of the total fibre CSA (*Figure* 4E and 4F). The presence of mMCAT fully restores the CSA of MHCIIb fibres in *Sod1*KO mice to the level measured in WT mice (*Figure* 4F).
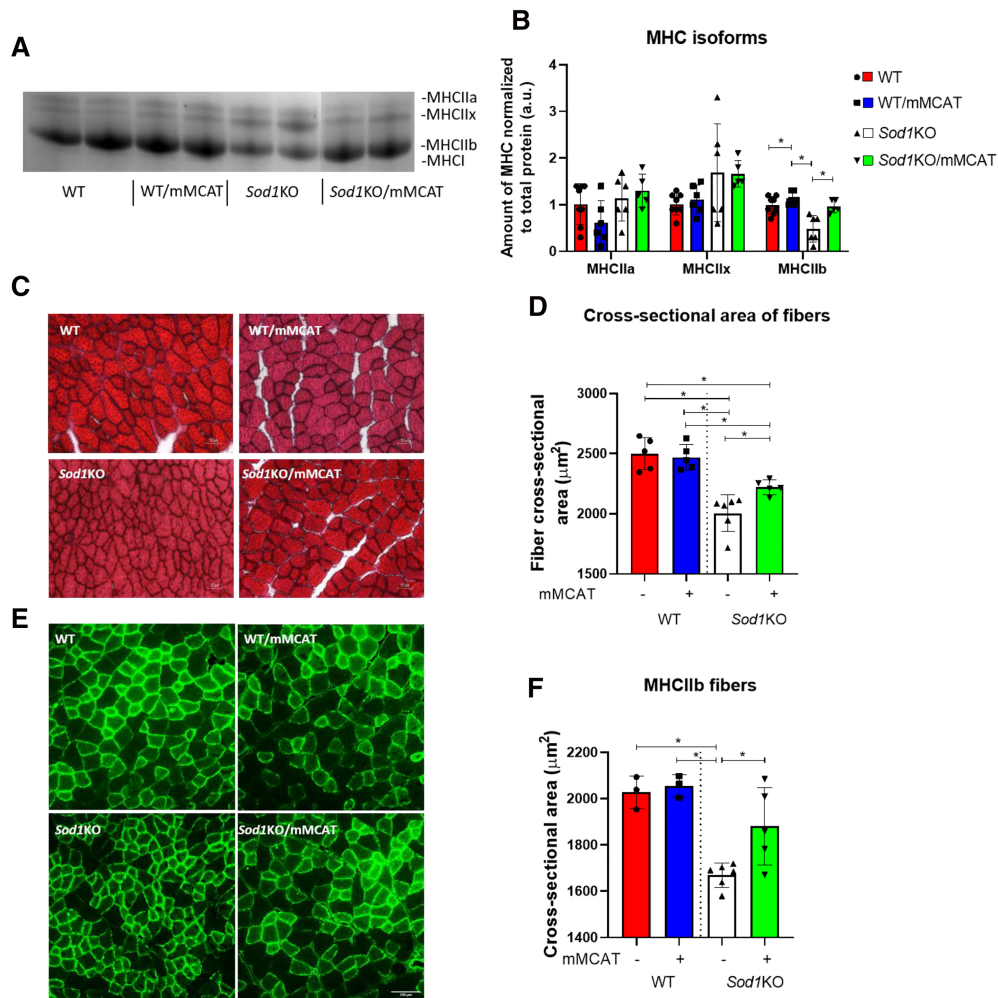
Figure 4 Muscle fibre size composition. (*A*) SDS-PAGE separation of MHC isoforms and (*B*) pooled data for each group. (*C*) H&E staining showing the total fibre cross-sectional area (CSA) along with (*D*) pooled data. (*E*) Immunostaining showing the fibres stained with MHCIIb antibody and (*F*) the pooled CSA data. *Significant difference between labelled groups (*P* < 0.05, one-way ANOVA). *N* = 5–8, indicating number of animals. Data are presented as mean ± standard deviation.

Force generation and the structure and function of neuromuscular junction (NMJ) are improved in *Sod1*KO mice by mMCAT expression

The muscle maximum specific force and the function of NMJ were measured using *in situ* electrical stimulation. In *Sod1*KO mice, in agreement with our previous work, we found that the maximum specific force (16 N/cm^2) is dramatically decreased compared with WT mice (25 N/cm^2). Strikingly, the expression of mMCAT in *Sod1*KO mice is associated with the restoration of force to a comparable level measured in WT mice (24 N/cm^2) (*Figure* 5A). The impact on NMJ function was determined by comparing the force generated using nerve stimulation through the NMJ to force generated by direct muscle stimulation, bypassing the NMJ. We found that the NMJ function in the *Sod1*KO mice is significantly

impaired, resulting in a ~30% functional denervation (i.e. nerve force/muscle force = 70%) (*Figure* 5B). In contrast, WT mice show a nerve/muscle directed force ratio close to 100%, indicative of full NMJ function (*Figure* 5B). With the expression of mMCAT, the nerve-induced force in *Sod1*KO mice is fully returned to 100% of the muscle-induced force, equivalent to WT mice (*Figure* 5B). The confocal microscopy images support these findings showing that the structure of the NMJ in *Sod1*KO mice is damaged with fragmentation and denervation, and mMCAT expression restores the NMJ in *Sod1*KO mice to a normal structure, which is similar to WT mice (*Figure* 5C). The quantification and statistical analysis indicate that in the *Sod1*KO mice, the NMJ area is smaller (722 μm^2) compared with WT mice (849 μm^2), the proportion of fragmented NMJ is remarkably higher (74%) than WT mice (11%), and the denervated NMJ proportion is extremely high
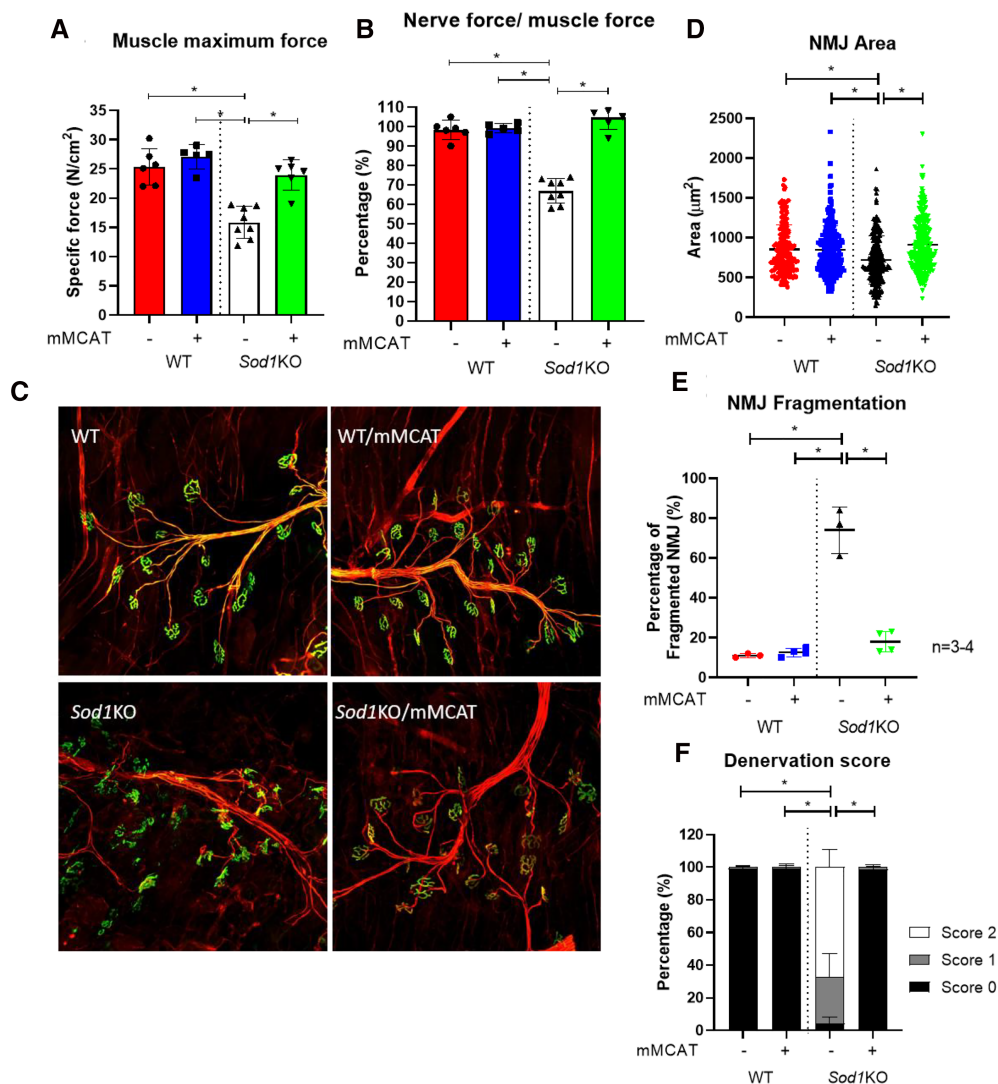
Figure 5 Muscle and NMJ function and morphology. (*A*) Specific muscle maximum force and (*B*) normalized proportion of the maximum nerve derived force to the maximum muscle derived force. (*C*) Representative confocal images for NMJ in different groups as labelled. (*D–F*) Pooled data for NMJ area, NMJ fragmentation, and denervation score of NMJ. *Significant difference between labelled groups (*P* < 0.05, one-way ANOVA). *N* = 3–4, indicating number of animals. Data are presented as mean ± standard deviation.

(96%) compared with WT mice (0.7%) (*Figure* 5D–5F). In the presence of mMCAT in the *Sod1*KO mice, all morphological NMJ parameters are similar to the WT mice; that is, the NMJ area is 909 μm^2, the fragmented NMJ is 18%, and the denervated NMJ is 1.2% (*Figure* 5D–5F).

The expression of mMCAT in Sod1KO mice restores SERCA activity

The activity of the SERCA pump, which is responsible for returning calcium to the SR following contraction and maintaining cytoplasmic calcium homeostasis, is sensitive to inactivation by oxidative stress,[20] potentially contributing to sarcopenia. *Figure* 6A shows SERCA activity in GTN muscle homogenates. In comparison with WT mice, both the maximum and the overall (area under activity curve) SERCA activity is dramatically reduced (~35%) in *Sod1*KO mice (*Figure* 6B and 6C). The reduction of SERCA activity in *Sod1*KO mice is completely reversed with the presence of mMCAT, showing no difference to WT mice (*Figure* 6B and 6C).

The expression of calcium-regulating proteins is altered in Sod1KO mice and restored to wildtype (WT) levels by the presence of mMCAT

Our previous work has shown that in addition to reduced SERCA activity, proteins involved in calcium homeostasis show altered expression in ageing and in muscle from

*Sod1*KO mice.[21] These changes can alter muscle metabolic pathways as well as EC coupling and contribute to sarcopenia. To determine whether mMCAT expression can modulate expression of calcium regulatory proteins, we measured protein abundance of calcium-regulating proteins in skeletal muscle, including the calcium storage protein inside SR, calsequestrin (CSQ1 and CSQ2), the SR transmembrane transport protein, SERCA (SERCA1 and SERCA2a), and the cytosolic calcium-binding and calcium-transporting protein, parvalbumin, using western blot analysis in whole muscle
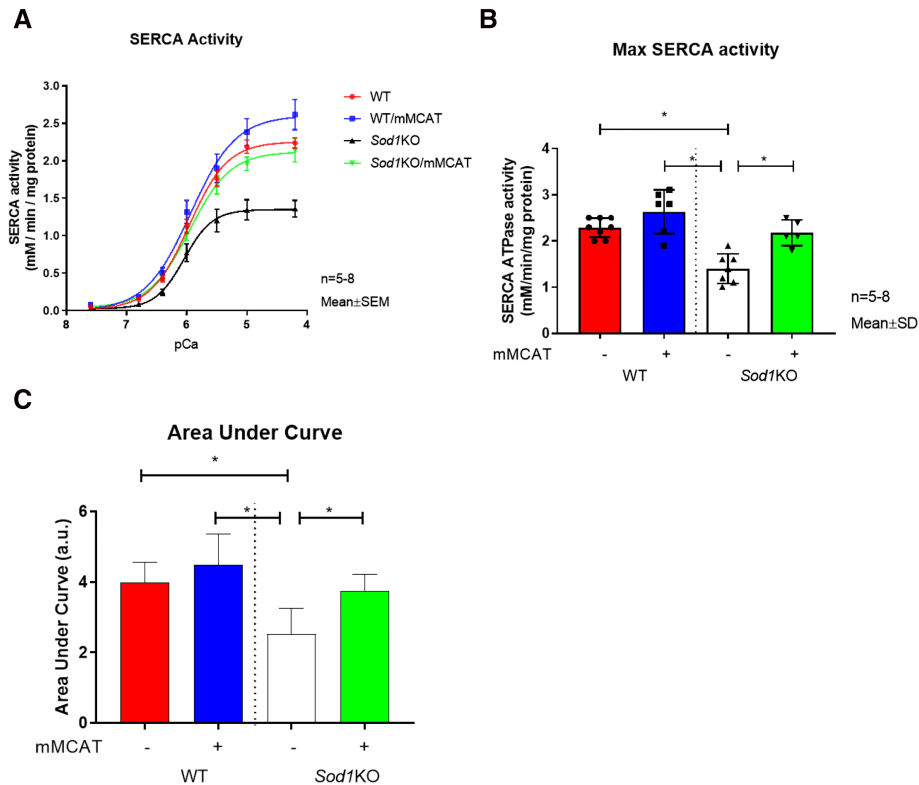
Figure 6 SERCA activity. (*A*) SERCA activity at different Ca^{2+} concentrations (pCa) and (*B*) pooled data of the area under curve and (*C*) the maximum SERCA activity. *Significant difference between labelled groups ($P < 0.05$, one-way ANOVA). N = 5–8, indicating number of animals. Data are presented as mean value ± standard deviation unless otherwise stated in the figure.
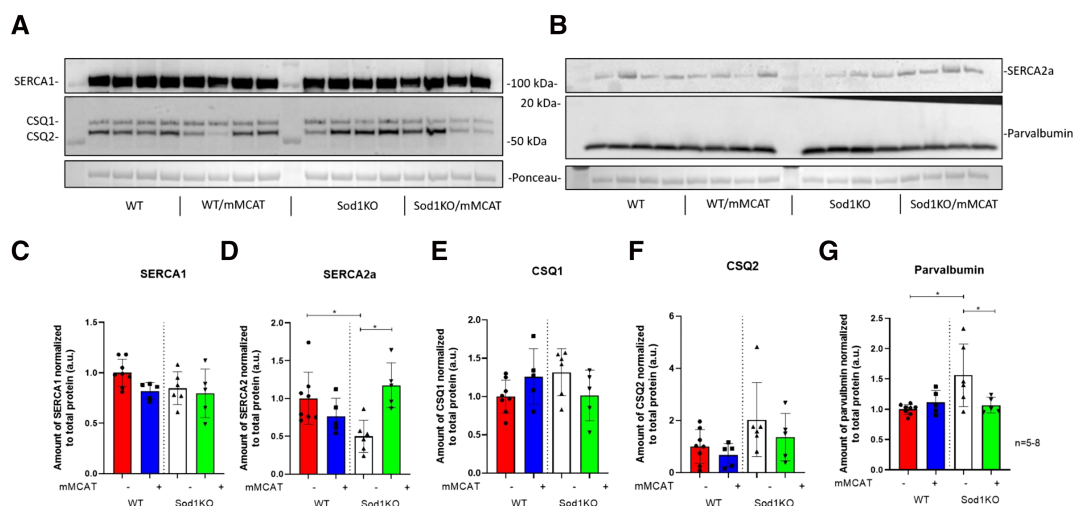
Figure 7 Amount of calcium-regulating proteins. Representative western blot (*A*) for SERCA1, CSQ1, and CSQ2 and (*B*) for SERCA2a and parvalbumin, and (*C*–*G*) pooled data for them respectively. *Significant difference between labelled groups ($P < 0.05$, one-way ANOVA). N = 5–8, indicating number of animals. Data are presented as mean value ± standard deviation.

homogenates. The abundance of both CSQ1 and CSQ2, as well as the fast isoform SERCA1, was stable across all four groups with no change (*Figure* 7A, 7C, 7E, and 7F). However, the amount of slow SERCA isoform, SERCA2a, was decreased for ~50% in *Sod1*KO mice compared with WT mice (*Figure* 7B and 7D), and this reduction was restored by the presence of mMCAT, showing no difference compared with WT mice (*Figure* 7D). Moreover, the deletion of *Sod1* also altered the expression of parvalbumin, and it was found that the amount of parvalbumin in *Sod1*KO mice increased significantly with 60% higher comparing with the WT mice (*Figure* 7B and 7G). The expression of mMCAT in *Sod1*KO mice reduced parvalbumin amount to that observed in WT mice (*Figure* 7G).

Discussion

The novel findings presented in this study show that the muscle-specific mitochondrial expression of catalase is sufficient to prevent the majority of muscle atrophy and weakness phenotypes present in the CuZnSOD null (*Sod1*KO) mouse model of oxidative stress-induced accelerated sarcopenia. Importantly, the expression of catalase localized specifically in skeletal muscle mitochondria (mMCAT) in the *Sod1*KO mice not only reduced hydrogen peroxide release by muscle mitochondria but also prevented the disruption of NMJ morphology and function that normally occurs in response to lack of CuZnSOD and elevated oxidative stress in the *Sod1*KO mouse model. These findings are important because they suggest a link between skeletal muscle mitochondria and the NMJ and a crosstalk between the muscle and motor neurons that can modulate skeletal muscle atrophy and weakness.

Mitochondria are a predominant site for the generation of superoxide anion, producing superoxide at complexes I and III, that is released to the mitochondrial matrix and intermembrane space.[22] The mitochondrial intermembrane space contains localized CuZnSOD (*Sod1*) that can scavenge superoxide generated from complex III, preventing superoxide release to the cytoplasm while contributing to increased potential H_2O_2 release to the cytosol, as well as potentially back into the mitochondrial matrix by diffusion. In the absence of CuZnSOD in the *Sod1*KO mice, superoxide generated at complex III may be released to the cytoplasm or potentially act to damage the electron transport chain causing mitochondrial dysfunction and further mitochondrial ROS generation. Conversely, superoxide released to the matrix from complexes I and III will be converted by MnSOD to H_2O_2 that is freely diffusible out of the mitochondrial matrix through the intermembrane space and out to the cytosol. The mitochondrial catalase, presumably in concert with the other mechanisms present to detoxify H_2O_2 such as peroxiredoxins and

glutathione peroxidase, can scavenge this H_2O_2, preventing damage to the electron transport chain or mitochondrial membranes and prevent its release to the cytosol, thus protecting both the mitochondria and the cell from increased oxidative stress. Consistent with this model, the whole-body MCAT mice have been reported to have a number of positive effects as a result of enhancing antioxidant activity of mitochondria.[8] In this study, we measured a number of indicators of mitochondrial function, including increased peroxide generation and reduced oxygen consumption, using permeabilized muscle fibres from WT, *Sod1*KO, and mMCAT*Sod1*KO mice. Mitochondrial proteins, in particular iron–sulfur centres of the respiratory enzymes (e.g. succinate dehydrogenase and NADH dehydrogenase), are specific targets of ROS and prone to oxidative modifications, potentially impacting the function of the electron transport chain and mitochondrial function.[22] Therefore, our results showing that scavenging the level of H_2O_2 in mitochondria by expression of catalase completely restored the reduction in OCR and generation of mitochondrial peroxide in muscle from *Sod1*KO mice to WT levels support the hypothesis that controlling H_2O_2 levels can maintain mitochondrial function.

The *Sod1*KO mice exhibit a number of age-dependent muscle atrophy phenotypes, such as lower muscle mass, and an altered body index with less fat mass that are likely caused in response to high oxidative stress.[4] In agreement with our previous findings, the results presented here show a similar effect on these parameters, as well as a reduction in running ability. Our results in this study also clearly confirm that the absence of *Sod1* leads to a reduction in maximum specific force and a disruption of NMJ structures, and a failure of neuromuscular transmission and NMJ function. The whole-body *Sod1* deletion likely increases mitochondrial ROS in both motor neurons and muscles, and the impairment of muscle and NMJ function is facilitated by compromised redox homeostasis.[23] Previously, we showed that replacing CuZnSOD in neurons in the *Sod1*KO mice prevents NMJ disruption and the deleterious muscle phenotypes in the *Sod1*KO mice.[24] The results we present here further demonstrate that expression of catalase restricted to muscle mitochondria can reduce muscle-specific mitochondrial ROS in the *Sod1*KO mice, preserving NMJ function and preventing muscle phenotypes as well. The NMJ fragmentation and increase in the percentage of denervated synapses in the *Sod1*KO mice are dramatically reversed by the expression of mitochondrial catalase in the *Sod1*KOxmMCAT mice. We saw a similar preservation of the NMJ and downstream muscle phenotypes in both ageing WT and *Sod1*KO mice maintained on dietary restriction.[25] The NMJ preservation was associated with reduced mitochondrial ROS generation and reduced oxidative damage, consistent with and antioxidant mechanism of protection. It is possible that H_2O_2 release in the *Sod1*KO mice results in alterations in NMJ-associated proteins, the local environment of the synapse, or even in the

motor neurons themselves through a muscle neuron retrograde pathway that can be reversed by increased expression of catalase and increased antioxidant protection. Fischer *et al*. found a similar preservation of the NMJ in a mouse model expressing human CuZnSOD targeted to the mitochondrial intermembrane space (mito*Sod1*) and crossed to the *Sod1*KO mice. Although the authors did not report changes in muscle mass, the expression of CuZnSOD in the mitochondrial intermembrane space was sufficient to prevent NMJ denervation in the *Sod1*KO mice up to 12 months of age and also prevented loss of grip strength.[26] The mito*Sod1* overexpression in this model was in several tissues including both neuronal and muscle tissues. These findings are consistent with our results indicating that reduced muscle mitochondrial oxidative stress may protect NMJ structure and function. Both muscle and nerve are highly metabolic and likely sensitive to changes in mitochondrial function that can alter metabolism. One potential candidate for retrograde communication between muscle and neurons is peroxisome proliferator-activated receptor gamma coactivator-1α (PGC-1α), which has been shown to mediate muscle nerve communication during activity and to control the expression of a number of NMJ-related proteins including AChRs, muscle-specific kinase, and utrophin.[27]

Muscle dysfunction can be associated with a number of potential factors, among them, an impairment in calcium regulation is considered to play a significant role.[28] One of the key enzymes in the calcium-regulating system is the SERCA, which executes the reuptake of cytoplasmic calcium into SR lumen maintaining the low Ca^{2+} concentration and protecting the contractile proteins after muscle contraction.[29] However, the SERCA pump is impaired in many chronic pathologies, including ageing,[30] muscular dystrophy,[31] and denervation,[32] and oxidative modification of SERCA has been reported as a potential underlying cause in the inactivation of SERCA pumps.[33] We have previously shown that *Sod1*KO mice have reduced SERCA activity in hindlimb skeletal muscle.[20] In the current study, we found that the expression of mMCAT fully restored SERCA activity in muscle from *Sod1*KO mice, suggesting that the reduction of hydrogen peroxide and oxidative stress by mMCAT efficiently protects SERCA function. It is probable that the restored SERCA activity contributes to the overall reduced atrophy and function phenotypes in the mMCAT × *Sod1*KO mice.

As a correlate to SERCA activity, we also measured the levels of calcium-regulating proteins such as SERCA, CSQ, and parvalbumin. SERCA and CSQ, two SR-related calcium-regulating proteins, both have two main different isoforms, with SERCA1 and CSQ1 being the fast isoform, and SERCA2a and CSQ2 being the slow isoform.[17] Our analysis showed that the amount of SERCA1 protein remained the same across all groups, supporting concept that the change in SERCA activity is not due to a change in protein abundance. In contrast, the amount of SERCA2a protein was decreased dramatically in

*Sod1*KO mice. The muscle used for this analysis was GTN muscle, which is almost entirely composed of fast-twitch fibres, and <5% of fibres are slow-twitch fibres.[34] SERCA2a is a slow isoform, and therefore, the change in the level of SERCA2a is not likely to contribute significantly to the activity change in GTN muscle. In addition, the MHC analysis in this study suggests that the reduction of SERCA2a is most likely due to the decreased abundance of the MHCI fibre type in *Sod1*KO mice. The amounts of both CSQ1 and CSQ2 proteins are stable across the different groups, indicating that the SR calcium storing ability is likely not affected by the elevated oxidative stress in *Sod1*KO mice. Interestingly, the abundance of parvalbumin was increased significantly in *Sod1*KO mice, with levels more than 50% higher than in WT mice, and the increase was reversed by expression of mMCAT. Parvalbumin is a cytosolic calcium/magnesium binding and buffering protein that facilitates the SR Ca^{2+} sequestration from cytosol side. In skeletal muscles, it is predominantly expressed in fast-twitch fibres where it functions to bind and transport calcium ions off from troponin C to SERCA during the relaxation. The expression of parvalbumin is therefore highly sensitive to the cytosolic Ca^{2+} concentration. It is possible that the elevated amount of parvalbumin in *Sod1*KO mice is attributable to the defect in SERCA function, resulting in increased cytosolic Ca^{2+} concentration or a prolonged clearance time for cytosolic Ca^{2+}, therefore increasing parvalbumin concentration. In addition, our previous findings also noted that the half-relaxation time is longer in *Sod1*KO mice,[20] suggesting a prolonged period of high of Ca^{2+} levels in the cytosol, which might also be responsible for the increased expression of parvalbumin. Taken together, the elevated expression of parvalbumin may be reversed by the restoration of SERCA activity, consistent with our findings in the *Sod1*KO mice with the presence of mMCAT.

In accordance to our previous findings, we described a phenotype in *Sod1*KO mice, in which the relative abundance of MHCIIb fibres is reduced compared with WT mice,[1] while other MHC isoforms are not affected. For this measurement, we used GTN muscle, a predominantly fast-twitch muscle consisting of predominantly fast-twitch fibres, MHCIIa, IIb, and IIx.[34] Previous studies have reported that type II fibres are more prone to ageing-induced atrophy,[1] and there is a tendency for fibre type switching from type II to type I fibres.[35] Here, we observed that only type IIb fibres are affected in the *Sod1*KO mice, not all type II fibres. In addition, we did not find conversion from type IIb fibres to other fibre types, rather we find a decrease in type IIb fibre diameter, suggesting that this is a fibre atrophy rather than a compositional change. The atrophy in type IIb fibres perfectly matches the decrease of the total CSA in whole muscle, supporting the fact that the total muscle atrophy is due primarily to the atrophy occurring in type IIb fibres. The potential underlying mechanism of this atrophy may be due to the regulating effects from PGC-1α.[36] It has been well

documented that PGC-1α is sensitive and up-regulated under the high oxidative stress environments, such as after highly intensive exercise,[37] and activated likely by phosphorylation of the PGC-1α protein by p38 MAPK together with NF-κB, with both of which are known to be activated by ROS.[38] PGC-1α plays a pivotal role on regulating muscle fibre compositions, by inhibiting the generation of glycolytic fibres (IIb/IIx) and promoting the synthesis of oxidative fibres (IIa/I).[39] Another potential mechanism could be the compromised muscle function in *Sod1*KO mice, where increased sedentary behaviour and reduced demand for activity may contribute to loss of the IIb fibres, the predominant active fibre type in rodent fast-twitch muscles.[17] The expression of mMCAT was highly effective in restoring the altered fibre composition in *Sod1*KO mice. This could be due to reduced impact of oxidative stress on PGC-1α and maintenance of the type IIb fibre size in *Sod1*KO mice. Although we did not measure spontaneous cage activity in the *Sod1*KO or *Sod1*KOxmMCAT mice, it is possible that MCAT expression may contribute indirectly to increased activity that along with maintained muscle contractile function may preserve the healthy fibre composition in *Sod1*KO mice. Notably, mMCAT expression did significantly improve the running ability in *Sod1*KO mice, although it remained lower than in WT mice. However, this is not necessarily surprising as treadmill running exercise is a complex whole-body network of actions that requires many other organs that are critical in running exercise, such as heart, artery, and lung functions. Finally, attributed to the restoration of the normal fibre contribution, the reduced muscle maximum specific force in *Sod1*KO mice is fully restored.

In summary, the results in this study clearly demonstrate that mitochondrial expression of catalase can prevent sarcopenia-like phenotypes induced by genetic deletion of *Sod1*, including muscle atrophy and weakness, NMJ disruption, inactivation of SERCA, mitochondrial defects, and a significant exercise intolerance. Our results clearly show that enhanced hydrogen peroxide scavenging potential in muscle mitochondria can maintain the NMJ structure and function in the *Sod1*KO mice and prevent the sequelae of events that occur downstream of loss of innervation to induce phenotypes associated with muscle atrophy and weakness in the *Sod1*KO mice. These finding support the importance of NMJ maintenance in sarcopenia.

Funding

Author contributions

H.X., A.R., and H.V.R. contributed in the conception and design of the research; H.X. and R.R. performed the experiments and analysed the data; H.X., A.R., and H.V.R. interpreted the results of the experiments; H.X. prepared the figures and drafted the manuscript; H.X., A.R., and H.V.R. edited and revised the manuscript; and H.X., R.R., A.R., and H.V.R. approved the final version of the manuscript.

Acknowledgements

Online supplementary material

Additional supporting information may be found online in the Supporting Information section at the end of the article.

Figure S1. oxphos coupling efficiency. Oxphos coupling efficiency (P-L control efficiency) of different groups (a). The relationship between P-L control efficiency and respiratory control ratio (RCR) published by Gnaiger E (2020) (Mitochondrial pathways and respiratory control. An introduction to OXPHOS analysis. 5th ed. Bioenerg Commun 2020.2: 112 pp). n = 6–10, indicating the number of animals. Data are presented as mean value ±standard deviation (SD).

Figure S2. Reactive oxygen species (ROS) production rate in isolated mitochondria. Reactive oxygen species (ROS) production rate of fibers with no substrate (State 1) is measured in isolated mitochondria. * indicates significant difference between the labelled groups ($P < 0.05$, One-Way ANOVA). n = 1–4, indicating the number of animals. Data are presented as mean value ±standard deviation (SD).

Figure S3. Detection of human catalase in different tissues in cytosolic and mitochondrial fractions. Reactive oxygen species (ROS) production rate in isolated mitochondria. Western blotting image shows the amount of human catalase in

cytosolic (Cyto) and mitochondrial (Mito) fractions from gastrocnemius muscle, liver, heart, and brain samples from both WT and mMCAT (Tg) mice. GAPDH and COXIV are used as representative protein markers for Cyto and Mito respectively. Note, the human catalase band in Tg Mito lane in gastroc sample is not lined up with the bands in liver and heart, those bands in liver and heart maybe the no-specific binding to mouse catalase, and also it shows no mitochondrial or transgenic specific.

Figure S4. Cytochrome c for testing the integrity of mitochondrial outer membrane in O2K technique. (a) is the representative respiratory curve for showing the oxygen consumption rate (OCR) with the addition of different substrates. In response to the addition of cytochrome c (CYC),

there is no increase seen with OCR, indicating no damage to the mitochondrial outer membrane. Abbreviations for the substrates: GM, glutamate and malate; ADP; SUC, succinate; CYC, cytochrome c; ROT, rotenone; AA, antimycin A; ASC/TMPD, ascorbate/N,N,N′,N′-Tetramethyl-p-phenylenediamine dihydrochloride. (b) is the quantified data of the OCR before and after the addition of cytochrome c.

Conflict of interest

None declared.

References

1. Jang YC, Lustgarten MS, Liu Y, Muller FL, Bhattacharya A, Liang H, et al. Increased superoxide *in vivo* accelerates age-associated muscle atrophy through mitochondrial dysfunction and neuromuscular junction degeneration. *FASEB J* 2010;**24**:1376–1390.

2. Arthur PG, Grounds MD, Shavlakadze T. Oxidative stress as a therapeutic target during muscle wasting: considering the complex interactions. *Curr Opin Clin Nutr Metab Care* 2008;**11**:408–416.

3. Martin GM, Loeb LA. Ageing: mice and mitochondria. *Nature* 2004;**429**:357–359.

4. Muller FL, Song W, Liu Y, Chaudhuri A, Pieke-Dahl S, Strong R, et al. Absence of CuZn superoxide dismutase leads to elevated oxidative stress and acceleration of age-dependent skeletal muscle atrophy. *Free Radic Biol Med* 2006;**40**:1993–2004.

5. Pharaoh G, Brown JL, Sataranatarajan K, Kneis P, Bian J, Ranjit R, et al. Targeting cPLA2 derived lipid hydroperoxides as a potential intervention for sarcopenia. *Sci Rep* 2020;**10**:13968.

6. Shahar S, Kamaruddin NS, Badrasawi M, Sakian NIM, Manaf ZA, Yassin Z, et al. Effectiveness of exercise and protein supplementation intervention on body composition, functional fitness, and oxidative stress among elderly Malays with sarcopenia. *Clin Interv Aging* 2013;**8**:1365.

7. Schriner SE, Linford NJ, Martin GM, Treuting P, Ogburn CE, Emond M, et al. Extension of murine life span by overexpression of catalase targeted to mitochondria. *Science* 2005;**308**:1909–1911.

8. Umanskaya A, Santulli G, Xie W, Andersson DC, Reiken SR, Marks AR. Genetically enhancing mitochondrial antioxidant activity improves muscle function in aging. *Proc Natl Acad Sci U S A* 2014;**111**: 15250–15255.

9. Dai DF, Johnson SC, Villarin JJ, Chin MT, Nieves-Cintrón M, Chen T, et al. Mitochondrial oxidative stress mediates angiotensin II-induced cardiac hypertrophy and Gαq overexpression-induced heart failure. *Circ Res* 2011;**108**:837–846.

10. Miniou P, Tiziano D, Frugier T, Roblot N, Le Meur M, Melki J. Gene targeting restricted to mouse striated muscle lineage. *Nucleic Acids Res* 1999;**27**:e27.

11. Larkin LM, Davis CS, Sims-Robinson C, Kostrominova TY, Van Remmen H, Richardson A, et al. Skeletal muscle weakness due to deficiency of CuZn-superoxide dismutase is associated with loss of functional innervation. *Am J Physiol Regul Integr Comp Physiol* 2011;**301**:R1400–R1407.

12. Ahn B, Ranjit R, Premkumar P, Pharaoh G, Piekarz KM, Matsuzaki S, et al. Mitochondrial oxidative stress impairs contractile function but paradoxically increases muscle mass via fibre branching. *J Cachexia Sarcopenia Muscle* 2019;**10**:411–428.

13. Krumschnabel G, Fontana-Ayoub M, Sumbalova Z, Heidler J, Gauper K, Fasching M, et al. Simultaneous high-resolution measurement of mitochondrial respiration and hydrogen peroxide production. *Methods Mol Biol* 2015;**1264**:245–261.

14. Gnaiger E. *Mitochondrial Pathways and Respiratory Control. An Introduction to OXPHOS Analysis*, 3rd ed. Innsbruck, Austria: Oroboros Instruments Corp.; 2012. 65.

15. Qaisar R, Pharaoh G, Bhaskaran S, Xu H, Ranjit R, Bian J, et al. Restoration of sarcoplasmic reticulum Ca^{2+} ATPase (SERCA) activity prevents age-related muscle atrophy and weakness in mice. *Int J Mol Sci* 2020;**22**:37.

16. Xu HY, Lamb GD, Murphy RM. Changes in contractile and metabolic parameters of skeletal muscle as rats age from 3 to 12 months. *J Muscle Res Cell Motil* 2017;**38**:405–420.

17. Xu H, Ren X, Lamb GD, Murphy RM. Physiological and biochemical characteristics of skeletal muscles in sedentary and active rats. *J Muscle Res Cell Motil* 2018;**39**:1–16.

18. Barker RG, Wyckelsma VL, Xu H, Murphy RM. Mitochondrial content is preserved throughout disease progression in the mdx mouse model of Duchenne muscular dystrophy, regardless of taurine supplementation. *Am J Physiol Cell Physiol* 2018;**314**:C483–C491.

19. Murphy RM, Xu H, Latchman H, Larkins NT, Gooley PR, Stapleton DI. Single fiber analyses of glycogen-related proteins reveal their differential association with glycogen in rat skeletal muscle. *Am J Physiol Cell Physiol* 2012;**303**:C1146–C1155.

20. Qaisar R, Bhaskaran S, Ranjit R, Sataranatarajan K, Premkumar P, Huseman K, et al. Restoration of SERCA ATPase prevents oxidative stress-related muscle atrophy and weakness. *Redox Biol* 2019;**20**:68–74.

21. Qaisar R, Bhaskaran S, Premkumar P, Ranjit R, Natarajan KS, Ahn B, et al. Oxidative stress-induced dysregulation of excitation–contraction coupling contributes to muscle weakness. *J Cachexia Sarcopenia Muscle* 2018;**9**:1003–1017.

22. Yan LJ, Levine RL, Sohal RS. Oxidative damage during aging targets mitochondrial aconitase. *Proc Natl Acad Sci U S A* 1997;**94**:11168–11172.

23. Deepa SS, Van Remmen H, Brooks SV, Faulkner JA, Larkin L, McArdle A, et al. Accelerated sarcopenia in Cu/Zn superoxide dismutase knockout mice. *Free Radic Biol Med* 2019;**132**:19–23.

24. Sakellariou GK, Davis CS, Shi Y, Ivannikov MV, Zhang Y, Vasilaki A, et al. Neuron-specific expression of CuZnSOD prevents the loss of muscle mass and function that occurs in homozygous CuZnSOD-knockout mice. *FASEB J* 2014;**28**:1666–1681.

25. Jang YC, Liu Y, Hayworth CR, Bhattacharya A, Lustgarten MS, Muller FL, et al. Dietary restriction attenuates age-associated

muscle atrophy by lowering oxidative stress in mice even in complete absence of CuZnSOD. *Aging Cell* 2012;**11**:770–782.

26. Fischer LR, Li Y, Asress SA, Jones DP, Glass JD. Absence of SOD1 leads to oxidative stress in peripheral nerve and causes a progressive distal motor axonopathy. *Exp Neurol* 2012;**233**:163–171.

27. Arnold AS, Gill J, Christe M, Ruiz R, McGuirk S, St-Pierre J, et al. Morphological and functional remodelling of the neuromuscular junction by skeletal muscle PGC-1α. *Nat Commun* 2014;**5**:3569.

28. Ali S, Garcia JM. Sarcopenia, cachexia and aging: diagnosis, mechanisms and therapeutic options—a mini-review. *Gerontology* 2014;**60**:294–305.

29. Lamboley CR, Murphy RM, McKenna MJ, Lamb GD. Sarcoplasmic reticulum Ca^{2+} uptake and leak properties, and SERCA isoform expression, in type I and type II fibres of human skeletal muscle. *J Physiol* 2014;**592**:1381–1395.

30. Thomas MM, Khan W, Betik AC, Wright KJ, Hepple RT. Initiating exercise training in late middle age minimally protects muscle contractile function and increases myocyte oxidative damage in senescent rats. *Exp Gerontol* 2010;**45**:856–867.

31. Voit A, Patel V, Pachon R, Shah V, Bakhutma M, Kohlbrenner E, et al. Reducing sarcolipin expression mitigates Duchenne muscular dystrophy and associated cardiomyopathy in mice. *Nat Commun* 2017;**8**:1068.

32. Dufresne SS, Dumont NA, Boulanger-Piette A, Fajardo VA, Gamu D, Kake-Guena S-A, et al. Muscle RANK is a key regulator of Ca^{2+} storage, SERCA activity, and function of fast-twitch skeletal muscles. *Am J Physiol Cell Physiol* 2016;**310**: C663–C672.

33. Dremina ES, Sharov VS, Davies MJ, Schöneich C. Oxidation and inactivation of SERCA by selective reaction of cysteine residues with amino acid peroxides. *Chem Res Toxicol* 2007;**20**:1462–1469.

34. Bloemberg D, Quadrilatero J. Rapid determination of myosin heavy chain expression in rat, mouse, and human skeletal muscle using multicolor immunofluorescence analysis. *PLoS ONE* 2012;**7**:e35273.

35. Holloszy JO, Chen M, Cartee GD, Young JC. Skeletal muscle atrophy in old rats: differential changes in the three fiber types. *Mech Ageing Dev* 1991;**60**:199–213.

36. Steinbacher P, Eckl P. Impact of oxidative stress on exercising skeletal muscle. *Biomolecules* 2015;**5**:356–377.

37. Kramer DK, Ahlsén M, Norrbom J, Jansson E, Hjeltnes N, Gustafsson T, et al. Human skeletal muscle fibre type variations correlate with PPARα, PPARδ and PGC-1α mRNA. *Acta Physiol* 2006;**188**:207–216.

38. Derbre F, Ferrando B, Gomez-Cabrera MC, Sanchis-Gomar F, Martinez-Bello VE, Olaso-Gonzalez G, et al. Inhibition of xanthine oxidase by allopurinol prevents skeletal muscle atrophy: role of p38 MAPKinase and E3 ubiquitin ligases. *PLoS ONE* 2012;**7**: e46668.

39. Lin J, Wu H, Tarr PT, Zhang C-Y, Wu Z, Boss O, et al. Transcriptional co-activator PGC-1α drives the formation of slow-twitch muscle fibres. *Nature* 2002;**418**:797–801.

40. von Haehling S, Morley JE, Coats AJS, Anker SD. Ethical guidelines for publishing in the Journal of Cachexia, Sarcopenia and Muscle: update 2019. *J Cachexia Sarcopenia Muscle* 2019;**10**:1143–1145.